JOURNAL OF RESEARCH of the National Bureau of Standards—A. Physics and Chemistry
Vol. 74A, No. 2, March–April 1970

Optical Properties and Electronic Density of States*[1]

Manuel Cardona[2]

Brown University, Providence, Rhode Island and DESY, Hamburg, Germany

(October 10, 1969)

The fundamental absorption spectrum of a solid yields information about critical points in the optical density of states. This information can be used to adjust parameters of the band structure. Once the adjusted band structure is known, the optical properties and the density of states can be generated by numerical integration. We review in this paper the parametrization techniques used for obtaining band structures suitable for density of states calculations. The calculated optical constants are compared with experimental results. The energy derivative of these optical constants is discussed in connection with results of modulated reflectance measurements. It is also shown that information about density of empty states can be obtained from optical experiments involving excitation from deep core levels to the conduction band.

A detailed comparison of the calculated one-electron optical line shapes with experiment reveals deviations which can be interpreted as exciton effects. The accumulating experimental evidence pointing in this direction is reviewed together with the existing theory of these effects.

A number of simple models for the complicated interband density of states of an insulator have been proposed. We review in particular the Penn model, which can be used to account for response functions at zero frequency, and the parabolic model, which can be used to account for the dispersion of response functions in the immediate vicinity of the fundamental absorption edge.

Key words: Critical points; density of states; dielectric constant; modulated reflectance; optical absorption.

1. Optical Properties and One-Electron Density of States

The optical behavior of semiconductors and insulators in the near infrared, visible, and ultraviolet is determined by electronic interband transitions. An additional intraband or free electron contribution to the optical properties has to be considered for metals. We shall discuss here the relationship between the interband contribution and the density of states. The interband contribution to the imaginary part of the dielectric constant can be written as (in atomic units, $\hbar=1$, $m=1$, $e=1$):

$$\epsilon_i(\omega)=\frac{1}{4\pi\omega}\iint_{\omega_{ef}=\omega}\frac{\mathbf{F}^{ef}}{|\nabla_{\mathbf{k}}\omega_{ef}|}dS_k \tag{1}$$

where $\omega_{ef}=\omega_e-\omega_f$ is the difference in energy between the empty bands (e) and the filled bands (f). The spin multiplicity must be included explicitly in eq (1). The oscillator strength tensor $\mathbf{F}^{ef}$ is related to the matrix elements of $\mathbf{p}$ through $\mathbf{F}^{ef}=2<f|\mathbf{p}|e><e|\mathbf{p}|f>\omega_{ef}^{-1}$. The Bloch functions are normalized over unit volume. Degenerate statistics has been assumed in eq (1) and spatial dispersion effects have been neglected.

It is customary to take the slowly varying oscillator strength out of the integral sign in eq (1) and thus write:

$$\epsilon_i(\omega)=\frac{2\pi^2}{\omega}\bar{F}N_d(\omega) \tag{2}$$

where $\bar{F}$ is an average oscillator strength and N_d the combined optical density of states.

Structure in $\epsilon_i(\omega)$ (eq (1)) appears in the neighborhood of critical points, where $\nabla_{\mathbf{k}}\omega_{ef}=0$. Such critical points can be localized in a small region of **k** space or can extend over large portions of the Brillouin zone over which filled and empty bands are parallel (sometimes only nearly parallel). Once the critical points which correspond to observed optical structure are identified in terms of the band structure through various devious and sometimes dubious arguments, their energies can

*An invited paper presented at the 3d Materials Research Symposium, *Electronic Density of States*, November 3–6, 1969, Gaithersburg, Md.

[1] Supported by the National Science Foundation and the Army Research Office, Durham.

[2] John Simon Guggenheim Foundation Fellow.

372-505 O - 70 - 8

be used to adjust parameters of semiempirical band structure calculations.

Four different parametric techniques of calculating band structures have been used for this purpose: the empirical pseudopotential method (EPM) [1], the $\mathbf{k} \cdot \mathbf{p}$ method [2], the Fourier expansion technique (FE) [3], and the adjustable orthogonalized plane waves method (AOPW) [4].

Once reasonably reliable band structures are known it is important to calculate from them the imaginary part of the dielectric constant $\epsilon_i(\omega)$ and to compare it with experimental results so as to confirm or disprove the initial tentative assignment of critical points and thus the accuracy of the band structures. Rich structure is obtained in both experimental and calculated spectra and hence a rather stringent test of the accuracy of the available theoretical band structure is in principle possible.

In order to calculate numerically the integral of eq (1) it is necessary to sample eigenvalues and eigenfunctions at a large number of points in the Brillouin zone. The amount of computer time required for solving the band structure problem with first-principles methods (OPW, APW, KKR) at a general point of the Brillouin zone makes such methods impractical for evaluating eq (1). The parametric methods (EPM, $\mathbf{k} \cdot \mathbf{p}$, FE, but not AOPW) require only the diagonalization of a small matrix (typically 30×30) and hence it is possible to sample the band structure at about 1000 points with only a few hours of computer time. Cubic materials, in particular those with T_d, O, and O_h point groups, are simple in this respect: symmetry reduces the sampling required for the evaluation of eq (1) to only 1/48 of the Brillouin zone. Hexagonal and tetragonal materials have relatively larger irreducible zones and hence a larger number of sampling points is necessary if the resolution of the calculation is not to suffer. Once the band structure problem has been solved for all points of a reasonably tight regular mesh, the bands and matrix elements at arbitrary points can be obtained by means of linear or quadratic interpolation.

The method of Gilat and coworkers [5] has become rather popular for the numerical evaluation of eq (1) [4,6]. In the case of a cubic material the Brillouin zone is divided into a cubic mesh and the band structure problem solved at the center of these cubes (sometimes a finer mesh is generated by quadratic interpolation from the coarser mesh [6]). Within each cube of the mesh the bands are linearly interpolated and approximated by their tangent planes. The areas of constant energy plane within each cube corresponding to a given ω_{ef} are added after multiplying them by the corresponding oscillator strength and thus the integral of eq (1) is obtained.

The real part of the dielectric constant ϵ_r can be obtained from ϵ_i by using the Kramers-Kronig relations. It is also possible to obtain ϵ_r and ϵ_i simultaneously by calculating the integral:

$$\epsilon(\omega) = 1 - \frac{1}{2\pi^2} \iiint \frac{\mathbf{F}^{ef}\omega_{ef}}{[\omega_{ef}^2 - (\omega + i\eta)^2]} \, dV_{\mathbf{k}} \qquad (3)$$

with η small and positive. For $\eta \rightarrow +o$ the imaginary part of eq (3) coincides with eq (1). Equation (3) can be evaluated with a Monte Carlo technique. Points are generated at random in $\mathbf{k}$ space within the Brillouin zone and the average value of the integrand for these points calculated. The process can be interrupted when reasonable convergence as a function of the number of random points is achieved [7,8].

We show in figure 1 the results of a calculation of ϵ_i from the $\mathbf{k} \cdot \mathbf{p}$ band structure of InAs with the method of Gilat and Raubenheimer [6]. The band structure problem, including spin-orbit effects, was solved at about 200 points of the reduced zone (1/48 of the BZ). We have indicated in this figure the symmetry of the critical points (or of the approximate regions of space) where the structure in ϵ_i originates. The experimental ϵ_i spectrum, as obtained from the Kramers-Kronig analysis of the normal incidence reflectivity [9], is also shown. The agreement between calculated and experimental spectra is good, with regards to both position and strength of the observed structure, with the excep-

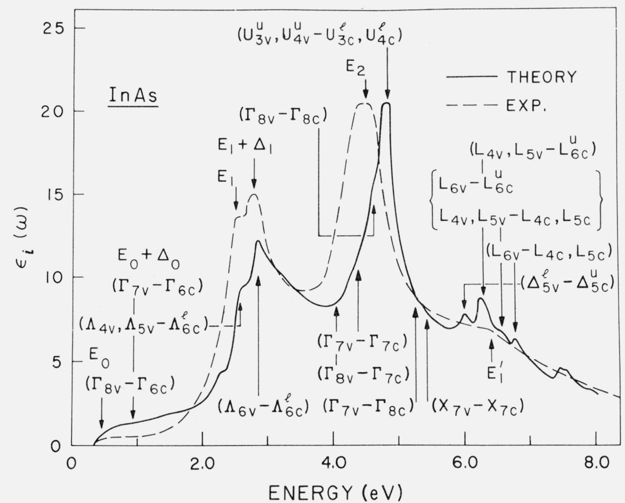

FIGURE 1. *Imaginary part of the dielectric constant of InAs as calculated from the* $\mathbf{k} \cdot \mathbf{p}$ *method* (——) [6] *and as determined experimentally* (----) [9]. *The group theoretical symmetry assignments were made with the help of the calculated isoenergy plots.*

tion of the position of the E_2 peak. This is to be attributed to an improper assignment of the E_2 peak when the 6 adjustable band structure parameters were determined. The E_2 peak had been attributed, following the tradition, to an X critical point while it is actually due to an extended region of **k** space centered around the U points [8]. It should be a simple matter to readjust the band structure parameters to lower the energy of the calculated E_2 peak by about 0.5 eV; in view of the large amount of computer time required to recalculate the energy bands this has not been done. The structure calculated around 6 eV, due mostly to spin-orbit splitting of the L_3 levels, has not yet been observed experimentally.

The conventional experimental determination of ϵ_i from normal incidence reflection data [9] suffers from considerable inaccuracy: to the experimental error produced by possible improper surface treatment and contamination one has to add the uncertainty in the high-energy extrapolation of the experimental data required for the Kramers-Kronig analysis. Some of these difficulties are avoided by comparing the *calculated* reflectivity spectra (obtained from ϵ with Fresnel's equation) with the experimental results. This is done in figure 2 for GaSb: the experimental data [10] have not been Kramers-Kronig analyzed because of the small range of the energy scale. Two calculated spectra have been plotted in this figure: one obtained from the $\mathbf{k} \cdot \mathbf{p}$ band structure [6] and the other obtained from a non-local pseudopotential calculation with 14 adjustable parameters [11]. The discrepancy between experimental and calculated curves at high energy, a common feature of many zincblende-type materials [12], has two origins: the measured reflectivity should be low because of increased diffuse reflectance at small wavelengths while the calculated one should be high because of the finite number of bands included in the calculation. In this region where $\epsilon_r - 1$ is small, the contribution to ϵ_r of transitions not included should lower the calculated reflectivity.

During the past few years a lot of activity has been devoted to the measurement and analysis of differential reflection spectra obtained with modulation techniques [13-15]. The wavelength (or photon energy) derivative spectra [14] should permit an accurate analysis of the line shapes of the spectra of figures 1 and 2. We show in figure 3 the temperature modulated reflection spectrum (thermoreflectance) of GaSb [15]: it has been shown that for the III–V materials [15] this spectrum is very similar to the photon energy derivative spectrum, difficult to obtain experimentally. The corresponding photon energy derivative spectrum obtained from the calculation of figure 2 is also shown in figure 3. The calculated and experimental shapes of the E_1, $E_1 + \Delta_1$ peaks show discrepancies of the type attributed in section 2 to exciton interaction. Derivative spectra for other germanium- and zincblende-type materials have been calculated by Walter and Cohen [12] and by Higginbotham [16].

The methods to calculate band structures from first principles, without or with only a few adjustable parameters (one [17] or three [4]) have recently achieved considerable success. However the calcula-

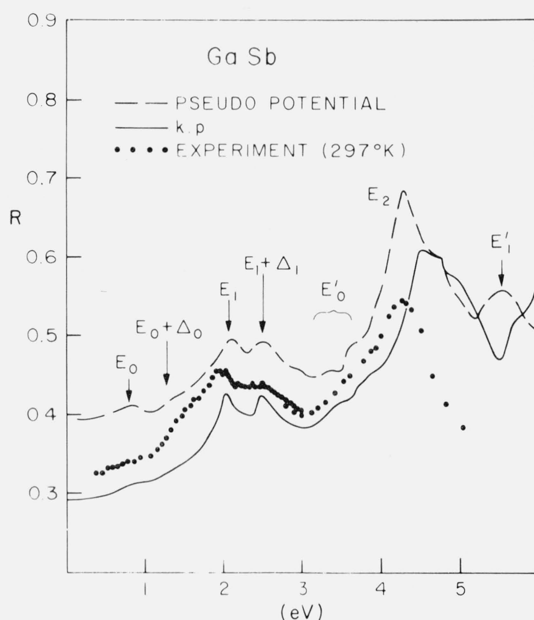

FIGURE 2. *Reflectivity of GaSb calculated from the* $\mathbf{k} \cdot \mathbf{p}$ *[6] and from a pseudopotential band structure [11]. Also, experimental reflectivity [10].*

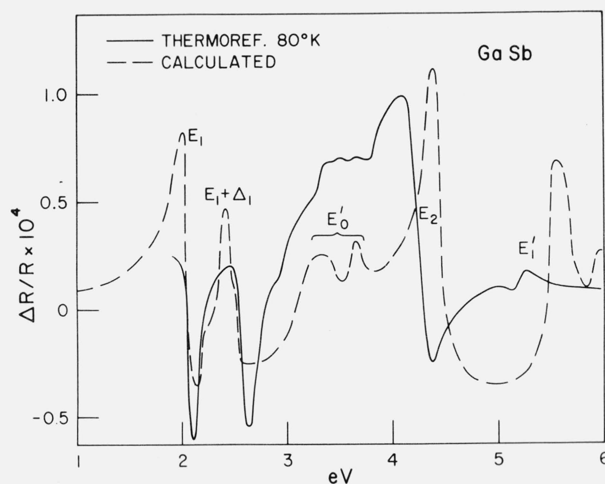

FIGURE 3. *Measured thermoreflectance spectrum of GaSb [15] compared with the energy derivative of the spectrum of figure 2 [16].*

tion of energy bands at one general point of the BZ requires a lot of time so as to make density of states calculations prohibitive. Moreover, the evaluation of the matrix elements required for eq (1) is difficult with first principles techniques. It is nevertheless possible to use first principles calculations at a few high-symmetry points of the Brillouin zone to adjust the parameters of semiempirical band structures from which the large number of sampling points required for the evaluation of eq (1) can be obtained with relative ease. The $\mathbf{k} \cdot \mathbf{p}$ technique has proved particularly useful in this respect [2,18,19]. Matrix elements of $\mathbf{p}$ can be easily evaluated from the eigenvectors in the $\mathbf{k} \cdot \mathbf{p}$ representation. Spin-orbit interaction can also be easily included. This $\mathbf{k} \cdot \mathbf{p}$ procedure has been applied to the relativistic OPW band structure calculated by Herman and Van Dyke for gray tin [19]. Figure 4 shows the reflectivity of gray tin calculated by this procedure with the method of Gilat and Raubenheimer together with experimental results [20]. Comparison with other experimental results for the germanium family suggests that the high-energy end of the measured spectrum is too low, probably due to surface imperfections in the delicate crystals, grown from mercury solution, which were used for this experiment.

The $\mathbf{k} \cdot \mathbf{p}$ fitting procedure has also been applied to a first principles relativistic APW calculation of the band structure of PbTe by Buss and Parada [7]. Figure 5 shows the reflectivity of PbTe obtained by this method with a Monte Carlo sampling technique and figure 6 the absorption coefficient, both compared with experimental data [7,21,22]. In both cases the semiquantitative agreement between experimental and calculated data is remarkably good in view of the absence of the adjustable parameters. The calculated reflectivity is, at high energies, considerably higher than the experimental one, as discussed earlier for other materials. The E_1 peak of the experimental reflectivity spectrum appears split in the calculated spectrum, possibly because of inaccuracies in the first-principles band structure. The calculated E_1 structure appears due mostly to transitions along the Σ direction. The experimental E_1 structure has been assigned [23] to the lowest gap along Σ. The calculated E_2 peak corresponds to an extended region of the BZ without definite symmetry, as inferred from electroreference measurements [23].

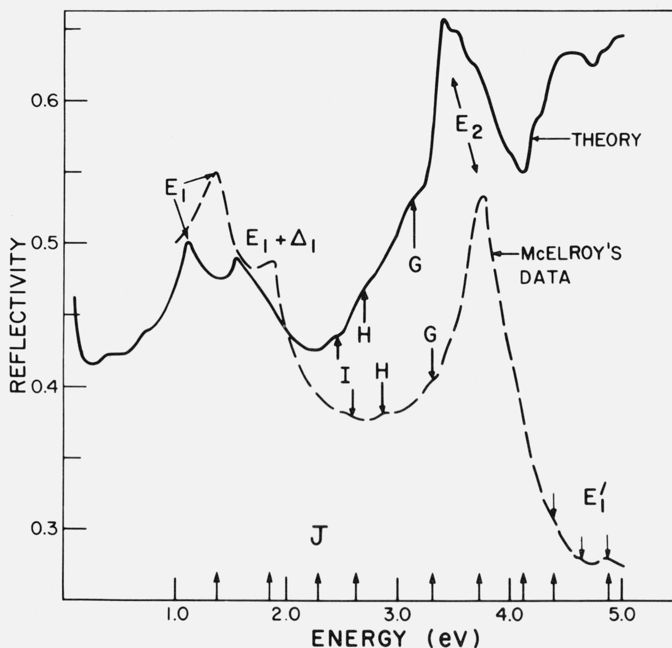

FIGURE 4. *Reflectivity of gray tin calculated from a first principles OPW band structure fitted with the* $\mathbf{k} \cdot \mathbf{p}$ *method [19]. Also experimental results [20].*

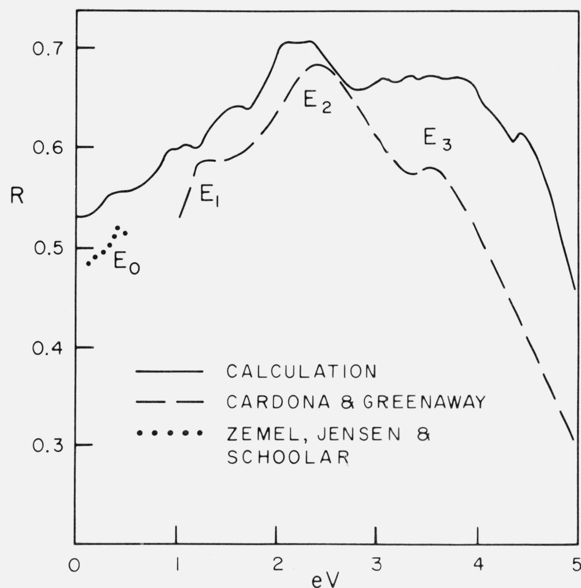

FIGURE 5. *Reflectivity of PbTe calculated from the APW-*$\mathbf{k} \cdot \mathbf{p}$ *band structure [7], compared with experimental results [21].*

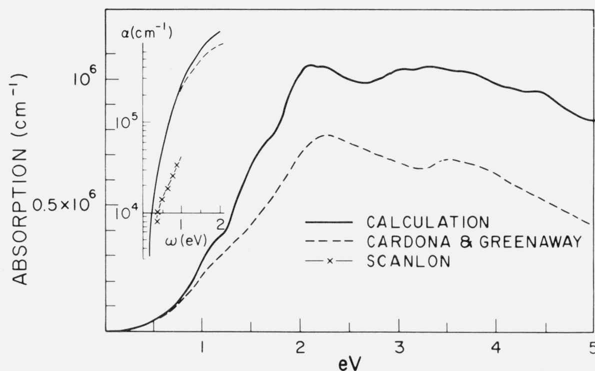

FIGURE 6. *Absorption coefficient PbTe calculated from the APW-*$\mathbf{k} \cdot \mathbf{p}$ *band structure, compared with experimental results [21, 22].*

We have so far discussed optical constants for cubic materials. While calculations for materials with lower symmetry require more computer time, one has the extra reward of being able to predict the experimentally observed anisotropy. Figure 7 shows the two principal components of ϵ_i for trigonal Se as calculated by Sandrock [24] from the pseudopotential band structure. The similarity between calculated and experimental results [25], also shown in figure 7, is especially remarkable in view of the method used to determine the pseudopotential parameters: they were determined from the pseudopotential parameters required to fit the optical structure of ZnSe. Only a small adjustment was performed so as to bring the calculated fundamental gap (1.4 eV) into agreement with the experimental one (2.0 eV). The dielectric constant of antimony (trigonal) for the ordinary and the extraordinary ray has also been calculated by a similar procedure [26].

The reasonable agreement obtained between experimental and calculated optical constants suggests the use of the corresponding band structure to determine the individual density of states $D(\omega)$: the main work, that of diagonalizing the Hamiltonian at a large number of points, has already been done. The programs required to calculate individual density of states are very similar to those used for the evaluation of eq (1): ω_{ef} must be replaced by the single band energies and $\mathbf{F}^{ef}$ must be removed. As an example we show in figure 8 the individual density of states of the 3 highest valence bands (six including spin) and the 3 lowest conduction bands of gray tin [19]. Direct information about the individual density of states can be obtained by a number of methods discussed in this conference. We mention, in particular, optical techniques involving transitions from deep core levels to the conduction band or from the valence band to temporarily empty core levels (soft x-ray emission) [27]. If the sometimes questionable assumption of constant matrix elements is made, the corresponding spectra represent the conduction (for absorption spectra) and the valence (for emission spectra) density of states because of the small width of the core bands. We show in figure 9 the densi-

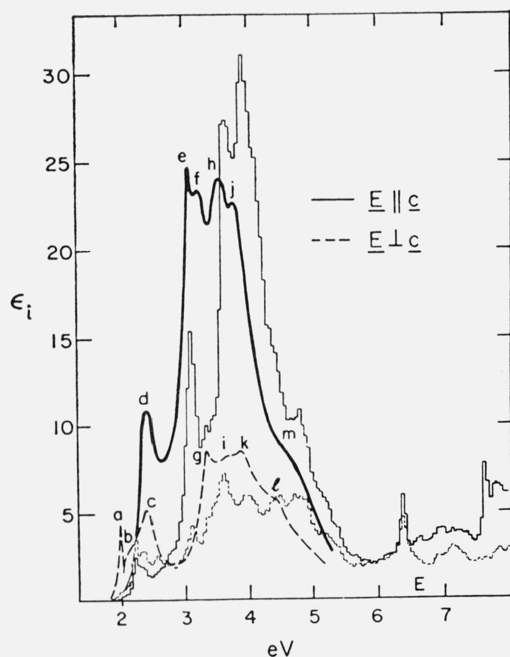

FIGURE 7. *Imaginary part of the dielectric constant of trigonal selenium for both principal directions of polarization of the electric field vector* **E** *as calculated from the pseudopotential band structure (histograms) [24] and as determined experimentally [25].*

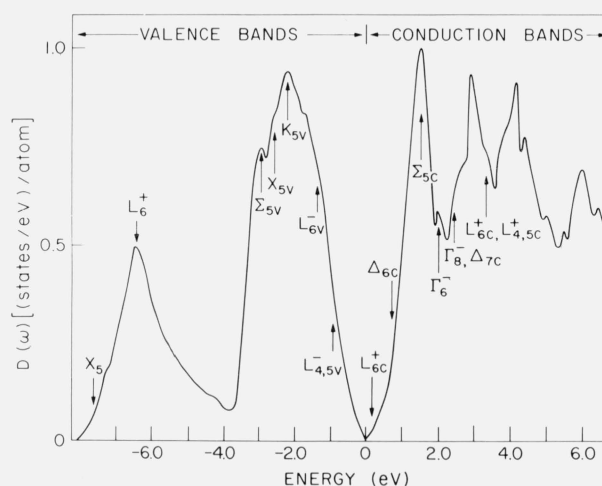

FIGURE 8. *Individual density of states for gray tin, obtained from the OPW-*$\mathbf{k}\cdot\mathbf{p}$ *band structure [19]. The top of the valence band is at 0 eV. The lowest valence band is not included.*

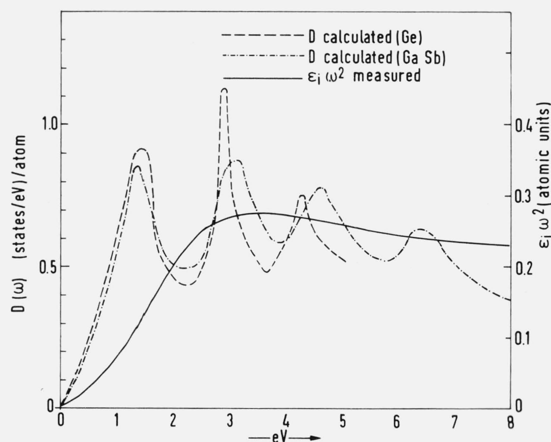

FIGURE 9. *Conduction density of states calculate for Ge [4] and for GaSb [6] together with the function* $\epsilon_i\omega^2$ *obtained from experimental data in the vacuum uv [28] (the horizontal scale for the* $\epsilon_i\omega^2$ *curve has been shifted by 29.5 eV).*

ty of states of the conduction band of Ge calculated by Herman, *et al.* [4] and the corresponding density of states for GaSb as obtained by the $\mathbf{k} \cdot \mathbf{p}$ method [6]. The densities of states for both materials are very similar because of the similarity of their band structures. We also show in figure 9 the quantity $\epsilon_i \omega^2$ obtained by Feuerbacher *et al.* [28] for Ge in the region of the $M_{4,5}$ edge. The origin of energies has been shifted so as to make a comparison with the conduction density of states possible: $\epsilon_i \omega^2$ should be proportional to $D(\omega)$ under the assumption of constant matrix elements of $\mathbf{p}$. While the rich structure of the calculated density of states is not seen in the $\epsilon_i \omega^2$ curve, this curve is reproduced quite well if the density of states is broadened so as to remove the fine structure. The required lifetime broadening of about 1 eV is not unreasonable for the $M_{4,5}$ transitions. Using eq (2) with N_d replaced by the conduction density of states we obtain an average oscillator strength at the maximum of $\epsilon_i \omega^2 \mathbf{F} = 0.15$. This oscillator strength corresponds to the 20 4d electrons per unit cell and hence it should be divided by 20 to obtain the average oscillator strength per d-band. If one reasons that the transitions from 10 of the 20 d bands to a given conduction band are forbidden because of the spin flip involved while transitions from 5 of these 10 bands are forbidden or nearly forbidden by parity, one finds for the average oscillator strength of each one of the 5 allowed bands $\overline{F} = 0.03$, which corresponds to a matrix element of $p = 0.13$ (in atomic units): this value is quite reasonable in view of the fact that the typical valence-conduction matrix element is 0.6. The small value of this matrix element explains why the d core electrons are negligible in the $\mathbf{k} \cdot \mathbf{p}$ analysis of the valence and conduction masses.

2. Exciton Effects

We have devoted section 1 to a comparison of experimental optical spectra with calculations based on the one-electron band structure. Exciton effects, *i.e.* the final state Coulomb interaction between the excited electron and the hole left behind, are known to modify substantially the fundamental edge of semiconductors and insulators [29]. Exciton-modified interband spectra seem also to occur in metals at interband edges which have the final state on the Fermi surface [30]. Experimental evidence for these effects is reported at this conference in the paper by Kunz *et al.*

We shall now discuss the question of exciton effects above the fundamental edge of insulators and semiconductors with special emphasis on the zincblende family. As mentioned in section 1 the gross features of these spectra are explained by the one-electron theory. The exciton interaction is responsible, at most, for small details concerning the observed line shapes. It is generally accepted [31,32] that the exciton interaction suppresses structure in the neighborhood of M_3 critical points: the Coulomb attraction with negative reduced masses is equivalent to a repulsion with positive masses. Such a repulsion smooths out critical point structure: no M_3 critical point has been conclusively identified in the experimental spectra. The E_1 and $E_1 + \Delta_1$ critical points of figures 1–3 are of the M_1 variety. Hence the line shape of the corresponding ϵ_i spectrum should be characterized by a steep low-energy side and a broader high-energy side. Figure 10 shows the shape of the E_1 peak observed at low temperature by Marple and Ehrenreich [33] and by Cardona [34]. In order to avoid effects due to the overlap of the E_1 and the $E_1 + \Delta_1$ peaks it has been assumed that they have exactly the same shape but shifted by 0.55 eV. The contribution of

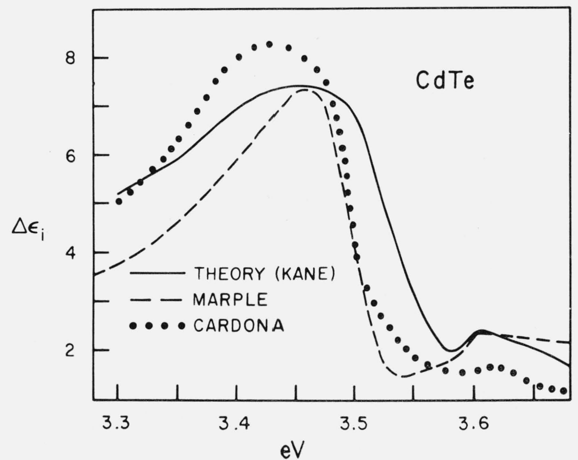

FIGURE 10. *Contribution of the* E_1 *gap to* ϵ_i *in CdTe as measured at low temperatures by Marple and Ehrenreich [33] and by Cardona [34]. Also calculation by Kane [32] using the adiabatic approximation.*

only E_1 has been extracted from the measured ϵ_i spectrum and displayed in figure 10. It is clear from this figure that the E_1 peak is steeper at high energies than at low energies, against the expectations for an M_1 peak. Also in figure 10 we show the results of a calculation by Kane [32] of the effect of Coulomb interaction on the E_1 line shape for CdTe, using the effective mass approximation. The solution of the effective mass Hamiltonian with non-positive-definite mass is made easier by the fact that the negative mass (along the Λ direction) has a magnitude much larger (about ten times) than the two equal positive masses. It is possible to use the adiabatic approximation [31], *i.e.*, to solve the two-dimensional hydrogen atom problem with the

third coordinate as a parameter and then solve the adiabatic equation for the third coordinate. The agreement between the calculated and the experimental line shapes of figure 10 is excellent.

Attempts have been made to calculate the dielectric constant including exciton interactions at an arbitrary point of **k** space, independently of the stringent restrictions of the effective mass approximation [35,36]. Such calculation is possible if one truncates the Coulomb interaction between electron and hole Wannier packets to extend to a finite number of neighboring cells. The extreme and simplest case of a δ-function (Koster-Slater) interaction can be solved by hand [31,35] and gives around an M_1 critical point the shapes of ϵ_r and ϵ_i shown in figure 11: for an M_i critical point the Koster-Slater interaction mixes the M_i one-electron line shape with the M_{i+1}. The high energy side of the ϵ_i peak becomes steeper, in agreement with figure 10. The line shape observed for the $E_1 - E_1 + \Delta_1$ peaks in the reflectivity spectrum is composed almost additively of the ϵ_i and ϵ_r line shape: at the energies of these peaks $dR/d\epsilon_i$ and $dR/d\epsilon_r$ are almost equal. We also show in figure 11 the line shapes expected for the reflectivity spectra of the $E_1 - E_1 + \Delta_1$ peaks and for the corresponding differential spectra ($dR/d\omega$). We show in figure 12 the photon energy derivative spectrum of these peaks in HgTe [37]: the observed line shapes disagree with those expected from the one-electron theory (equal positive and negative peaks) but agree with those predicted in the presence of a Koster-Slater interaction (fig. 11). Similar results have been found for other zincblende-type materials [37].

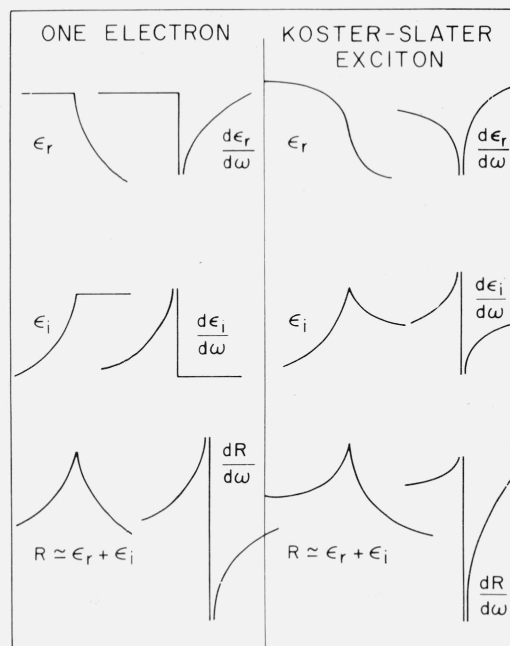

FIGURE 11. *Modification in ϵ_r and ϵ_i introduced by the Koster-Slater exciton interaction in the neighborhood of an M_1 critical point. Also, effect on the reflectivity under the assumption of an equal contribution of $\Delta\epsilon_r$ and $\Delta\epsilon_i$ to the reflectivity line shape.*

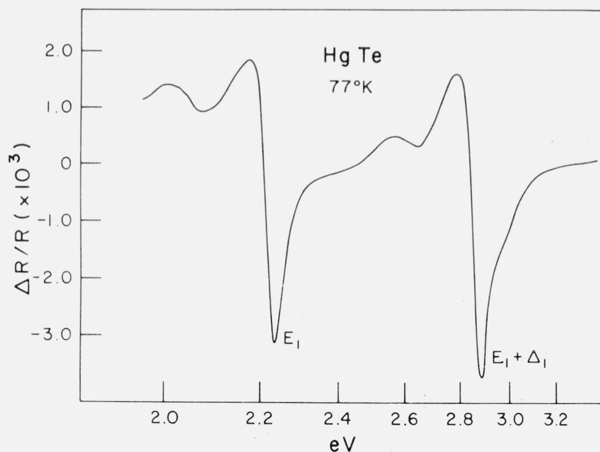

FIGURE 12. *Photon energy derivative spectrum of the reflectivity of HgTe in the neighborhood of the E_1 and $E_1 + \Delta_1$ structure [37].*

3. Simplified Models for the Density of States

As seen in section 1 the optical density of states, and thus the dielectric constant, is a complicated function of frequency and its calculation requires lengthy numerical computation. For some purposes, however, it can be approximated by simple functions. In the vicinity of a critical point of the M_i variety, for instance, the singular behavior of the dielectric constant can be approximated by:

$$\epsilon \propto i^{r+1}(\omega - \omega_g)^{1/2} + \text{constant} \qquad (4)$$

if exciton effects are neglected. Exciton interaction can be included, within the Koster-Slater model, by multiplying eq (4) by a phase factor $e^{i\phi}$ with ϕ small and positive.

As shown in figure 1, ϵ_i for the zincblende-type materials has a strong peak (E_2) in the neighborhood of which most of the optical density of states is concentrated. The corresponding transitions occur over a large region of the BZ, close to its boundaries. In order to represent this fact, Penn [38] suggested the model of a non-physical spherical BZ with an isotropic gap at its boundaries. The complex energy bands of the material are then replaced by those of a free electron with an isotropic gas ω_g at the boundary of a spherical BZ. This gap should occur in the vicinity of the E_2 optical structure. While this model represents rather poorly the rich

structure of ϵ_i (fig. 1), it is expected that it should give a good picture of ϵ_r at zero frequency. The reshuffling of density of states involved in the case of the isotropic model should not affect $\epsilon_r(\omega = o)$ very much because of the large energy denominators which appear in eq (3) for $\omega = o$: the lowest gap ω_o, usually much smaller than ω_g, accounts only for a very small fraction of the optical density of states. Penn obtained with this model the static dielectric constant for a finite wavevector $\mathbf{q}$. The result can be approximated by the analytic expression [38]:

$$\epsilon(\omega = o, q) = 1 + \left(\frac{\omega_p}{\omega_g}\right)^2 \mathscr{F} \left\{1 + \frac{\omega_F}{\omega_g} \frac{q}{k_F} \mathscr{F}^{1/2}\right\}^{-2} \quad (5)$$

with
$$\mathscr{F} = 1 - \frac{\omega_g}{4\omega_F} + \frac{1}{3}\left(\frac{\omega_g}{\omega_F}\right)^2$$

In eq (5) ω_p is the plasma frequency obtained for the density of valence electrons and ω_F and k_F the corresponding free electron Fermi energy and wave number. The dimensionless quantity $\mathscr{F}$ is usually close to one.

Figure 13 shows eq (5) for Si compared with the exact results of the Penn model [39]. These results are obviously independent of the direction of $\mathbf{q}$. A small dependence on this direction is found from a complete pseudopotential calculation by Nara [40] (see also fig. 13). The function $\epsilon(o, \mathbf{q})$ is of interest for the treatment of dielectric screening.

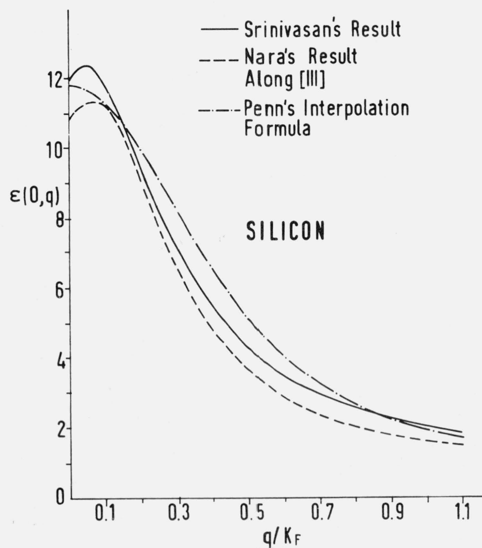

FIGURE 13. *Static dielectric constant $\epsilon(o, \mathbf{q})$ obtained by Srinivasan [39] for Si with the Penn model compared with the interpolation formula of eq (5) and with the results of a pseudopotential calculation by Nara [40] for $\mathbf{q}$ along (111).*

Equation (5) yields for $\mathbf{q} = o$ the electronic contribution to the static dielectric constant:

$$\epsilon_o = 1 + \mathscr{F}\left(\frac{\omega_p}{\omega_g}\right)^2 \simeq 1 + \left(\frac{\omega_p}{\omega_g}\right)^2 \quad (6)$$

The experimental values of ϵ_o agree reasonably well with the results of eq (6) using for ω_g the energy of the E_2 peak [34]. Equation 6 has gained recent interest as the basis of Phillips and Van Vechten's theory of covalent bonding [41,42,43]. These authors use eq (6) and the experimental values of ϵ_o to define the average gap ω_g. With this gap and the corresponding gap of the isoelectronic group IV material they can interpret a wide range of properties such as crystal structure [42], binding energy [43], energies of interband critical points [41], non-linear susceptibilities [44], *etc.* As an example we discuss the hydrostatic pressure (*i.e.* volume) dependence of ϵ_o for germanium and silicon. According to Van Vechten [41], ω_g for C, Ge, Si, and $\alpha-$Sn is proportional to $(a_o)^{-2.5}$ where a_o is the lattice constant. If one makes the assumption that this law gives also the change in ω_g with lattice constant for a given material when hydrostatic stress is applied one can calculate the volume dependence of ϵ_o [41]. Neglecting the one in eq (6), a valid approximation for Ge and Si, one finds:

$$\frac{1}{\epsilon_o}\frac{d\epsilon_o}{dV} = 2\left(\frac{d \ln \omega_p}{dV} - \frac{d \ln \omega_g}{dV}\right)$$

$$= 2[0.83 - 0.50] = 0.66 \quad (7)$$

Equation (7) explains the sign and the small magnitude observed for $(1/\epsilon_o)(d\epsilon_o/dV)$. The experimental values of this quantity are 1.0 for Ge and 0.6 for Si [41,45].

According to eq (6) the average gap ω_g determines the electronic dielectric constant for $\omega = o$. As the lowest gap ω_o is approached ($\omega_o \ll \omega_g$ usually), ϵ_r exhibits strong dispersion. This dispersion is due, in the spirit of eq (3), to the density of states in the vicinity of ω_o. For the purpose of calculating the dispersion of ϵ_r immediately below ω_o, the density of states can be approximated by that of parabolic bands with a reduced mass equal to the reduced mass μ at ω_o. These bands are assumed to extend to infinity in $\mathbf{k}$ space: the unphysical contribution to ϵ_r for $|k| \to \infty$ should be small for $\omega \leqslant \omega_o$, because of the large energy denominators of eq (3). We thus obtain for a cubic material the following contribution of the ω_o gap to the scalar dielectric constant below ω_o (under the assumption of a constant matrix element of $\mathbf{p}$ equal to $\mathbf{P}$) [46]:

$$\Delta\epsilon_r = 2(2\mu)^{3/2}\omega_0^{3/2}|P|^2 f(\omega/\omega_0) = C_0'' f(\omega/\omega_0)$$

with (8)

$$f(x) = 2 - (1+x)^{1/2} - (1-x)^{1/2}.$$

Equation (8) represents quite well the behavior of ϵ_r immediately below ω_o for the lead chalcogenides [47] and a number of other semiconductors [48]. As an example we show in figure 14 the observed dispersion of ϵ_r below ω_o at room temperature [49] together with a fit based on eq (8) [48]. For the sake of completeness we have included in the fitting equations not only the effect of ω_o (E_o) but also that of its spin-orbit-split mate $E_o + \Delta_o$ (also represented by an expression similar to eq (8)), the dispersion due to the E_1 and $E_1 + \Delta_1$ gaps, and that due to the main ω_g gap assuming $\omega_g \equiv E_2$. Thus the fitting equation with three adjustable parameters C_0'', C_1'', C_2'' is [48]:

$$\epsilon_r(\omega) = 1 + C_o''\left\{f(x_o) + \frac{1}{2}\left(\frac{\omega_o}{\omega_{os}}\right)^{3/2} f(x_{os})\right\} \qquad (9)$$

$$+ C_1''\left\{h(x_1) + \left(\frac{\omega_1}{\omega_{1s}}\right) h(x_{1s})\right\} + C_2''(1 + 2x_2^2)$$

where:

$$\omega_{os} = \omega_o + \Delta_o, \qquad x_{os} = \frac{\omega}{\omega_{os}}, \qquad x_1 = \frac{\omega}{\omega_1}$$

$$\omega_{1s} = \omega_1 + \Delta_1, \qquad x_{1s} = \frac{\omega}{\omega_{1s}}, \qquad x_2 = \frac{\omega}{\omega_g}$$

$$h(x_1) = 1 + \frac{x_1^2}{2}.$$

The fitting values of C_0'' (6.602) and C_1'' (2.791) are in qualitative agreement with those calculated from the band parameters [48].

The parabolic model density of states can also be used to interpret the strong dispersion in the piezobirefringence observed near the lowest direct gap of

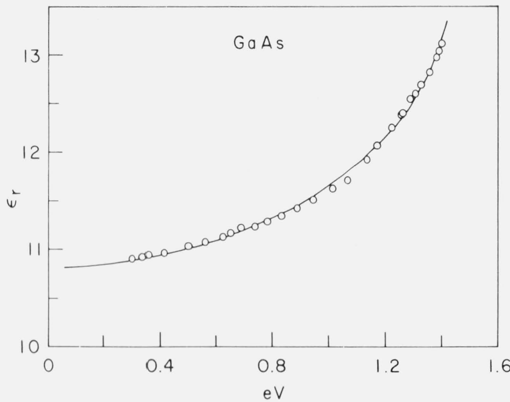

FIGURE 14. *Experimental results for ϵ_r in GaAs below the fundamental edge at room temperature [49] (circles) and fitted curve based on a model density of states.*

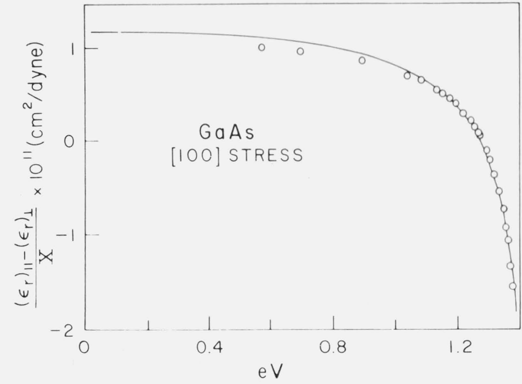

FIGURE 15. *Piezobirefringence in GaAs for an extensive stress along (100) (room temperature). The circles are experimental points. The solid line is a fit based on the model of eq (5) [48].*

Ge, GaAs [48], and other III−V semiconductors [50,51]: uniaxial stress splits the top valence band state (Γ_8) and a birefringence in the contribution of E_o to ϵ_r results because of the selection rules for transitions from the split bands. The main contribution to this piezobirefringence is expected to be proportional to f′(x), which diverges like $(\omega - \omega_0)^{-1/2}$ for $\omega \rightarrow \omega_o$. Such behavior can be seen in the experimental results (circles) of figure 15 obtained for GaAs at room temperature. Included in this figure is the corresponding fit based on the model of eq (9) [48].

The long wavelength, non-dispersive contribution to the piezobirefringence of figure 15 can be interpreted, at least qualitatively, in terms of the Penn model of eqs (6) and (7). Equation (7) yields two contributions to the change in ϵ_r one due to the change in plasma frequency (*i.e.* carrier density) with stress and the other due to the change in the isotropic gap. The first contribution should not exist for a pure shear stress. For a hydrostatic stress the second contribution can be written in tensor form as:

$$\frac{1}{\epsilon_0}\Delta\boldsymbol{\epsilon}_0 = 5\mathbf{e} \qquad (10)$$

where **e** is the strain tensor. We postulate that eq (8) remains valid for pure sheer stress. This crude generalization has a clear physical meaning in terms of the Penn model. The spherical BZ becomes ellipsoidal under a sheer stress and the energy gap at an arbitrary point of the BZ boundary k_F becomes anisotropic. The gap at k_F is assumed to become larger as k_F becomes larger (k_F is the distance between atomic planes per-

pendicular to k_F). Equation (8) gives the right sign for the long wavelength contribution to the piezobirefringence of figure 15 but a magnitude about five times larger. The agreement becomes better if the contribution of the E_0 edge to the long wavelength piezobirefringence, of opposite sign to that predicted by eq (10), is subtracted from the experimental results.

4. Third Order Susceptibility and Model Density of States

It has been recently suggested [52] that the third order susceptibility of Ge, Si, and GaAs at long wavelengths is related to the Franz-Keldysh effect (*i.e.* the intraband coupling by the field) of interband critical points [53]. We discuss now the Franz-Keldysh contribution of the ω_g, E_0, and E_1 gaps to $\chi^{(3)}_{1111}$.

4.1. Average Gap ω_g

In the spirit of Penn's model [38] we represent the long-wavelength dielectric constant by eq (6) with $\mathscr{F}=1$. The corresponding imaginary part of the dielectric constant is, for $\omega > \omega_g$ [47]:

$$\epsilon_i = A^{-2}(\omega-\omega_g)^{-1/2}$$

with

$$A=\frac{4}{3}\,\omega_p^2\omega_g^{1/2} \tag{11}$$

The Franz-Keldysh effect for the one-dimensional absorption edge of eq (11) can be expressed in terms of the Airy functions Ai and Bi [54]. One must mention, however, that the isotropic gap problem in the presence of an electric field would only be completely equivalent to the one-dimensional problem if the field experienced by every electron were along the direction of the corresponding **k**. The fact that the field $\mathscr{E}$ is the same for all electrons, regardless of **k**, can be taken into account by using an average field:

$$\langle \mathscr{E}^2\rangle = \frac{\langle \cos^4\beta\rangle}{\langle\cos^2\beta\rangle}\mathscr{E}^2=\frac{3}{5}\mathscr{E}^2 \tag{12}$$

where β is the angle between **k** and $\mathscr{E}$. The long-wavelength expression for $\chi^{(3)}_{1111}$ thus is [54]:

$$\chi^{(3)}_{1111}=\frac{3A}{20\pi\omega^2}\lim_{\substack{\mathscr{E}\to 0\\ \omega\to 0}}\mathscr{E}^{-2}\theta^{-1/2}\left(G_1\left(\frac{\omega_g+\omega}{\theta}\right)+G_1\left(\frac{\omega_g-\omega}{\theta}\right)-G_1\left(\frac{\omega_g}{\theta}\right)\right), \tag{13}$$

where the one-dimensional electro-optic function $G_1(\eta)$ is given by [54]:

$$G_1(\eta)=2\pi Ai(\eta)Bi(\eta)-H(\eta)\eta^{-1/2}$$

$$\theta=\left(\frac{\mathscr{E}^2}{2\mu}\right)^{1/3} \tag{14}$$

In eq (14) H (η) is the unit step function and μ the reduced mass of the Penn model, given by $\mu=\omega_g(2k_F)^{-2}$. The Fermi momentum of the valence electrons is related to the plasma frequency ω_p through $k_F^3=(3/4)\pi\omega_p^2$.

The limit for $\mathscr{E}\to 0$ in eq (14) is easily found using the asymptotic expansions of Ai (η) and Bi (η) for $\eta\to+\infty$ [55]. By subsequently performing the limit for $\omega\to 0$ one finds:

$$\chi^{(3)}_{1111}=\frac{287}{256\pi}\left(\frac{3}{4}\pi\right)^{2/3}(\epsilon_o-1)\frac{\omega_p^{4/3}}{\omega_g^4} \tag{15}$$

Or, for ease of evaluation, with $\chi^{(3)}_{1111}$ in e.s.u., and the energies in eV:

$$\chi^{(3)}_{1111}=1.45\cdot 10^{-11}(\mathscr{E}_o-1)\frac{\omega_p^{4/3}}{\omega_g^4} \tag{16}$$

We list in table I the values of ω_g, ω_p and ϵ_o-1 for Ge, Si and GaAs. The values of $\chi^{(3)}_{1111}$ calculated with eq (16) are then listed in table II. This table shows agreement in sign and magnitude between the values of $\chi^{(3)}_{1111}$ predicted from ω_g and the experimental ones. An increase in the polarizability with field ($\chi^{(3)}_{1111}>0$) is to be expected for the Franz-Keldysh effect since the intraband coupling by the electric field produces a decrease in the energy gap.

We shall consider now the contribution to $\chi^{(3)}_{1111}$ of the interband coupling by the electric field across the isotropic gap ω_g. This coupling produces an increase in energy gap, and thus its contribution to $\chi^{(3)}_{1111}$ is negative. This contribution to $\chi^{(3)}_{1111}$ is readily found from eq (6):

$$\Delta\chi^{(3)}_{1111}=-\frac{3}{5\pi}(\epsilon_o-1)\frac{1}{\omega_g}\frac{d\omega_g}{d(\mathscr{E}^2)}$$

$$=-\frac{3(\epsilon_0-1)}{5\pi}\left(\frac{3\pi}{4}\right)^{2/3}\frac{\omega_p^{4/3}}{\omega_g^2} \tag{17}$$

In eq (17) we have made use of the second-order perturbation expression:

$$\frac{d\omega_g}{d(\mathscr{E}^2)}=2\frac{|\langle v|\mathbf{r}|c\rangle|^2}{\omega_g}=\frac{2k_F^2}{\omega_g^2} \tag{18}$$

Equation (18) is in agreement with the results of ref. [44]. Comparison of this equation with eq (15) shows that the magnitude of the interband contribution to $\chi^{(3)}_{1111}$ differs from that of the intraband contribution by a factor of order $\omega_g{}^2$ (ω_g in atomic units). It is therefore almost two orders of magnitude smaller and hence negligible.

4.2. Lowest Gap E_0

We use for the contribution of an isotropic M_0 critical point to the real part of the dielectric constant the result of eq (8). A calculation similar to that performed above yields for an M_0 critical point the following Franz-Keldysh contribution to $\chi^{(3)}_{1111}$ [52]:

$$\Delta\chi^{(3)}_{1111}=0.06\frac{p^2\mu_o^{1/2}}{\omega_0^{9/2}}\left(1+1.85\left(\frac{\omega}{\omega_o}\right)^2+. . .\right) \quad (19)$$

or, transforming $\Delta\chi^{(3)}_{1111}$ to e.s.u. and ω_o to eV (P^2 and μ_o are left in atomic units for ease of computation):

$$\Delta\chi^{(3)}_{1111}(\omega)=6\cdot 10^{-10}\frac{C_0^2\mu_0^{1/2}}{\omega_0^{9/2}}\times\left(1+1.85\left(\frac{\omega}{\omega_o}\right)^2+. . .\right) \quad (20)$$

We have included in eqs (19) and (20) the first term in the dispersion of $\Delta\chi^{(3)}_{1111}$ since it may be possible to observe it experimentally in small band gap materials. This dispersion is given exactly by the function:

$$\frac{\omega_0^2}{\omega^2}\left(\left(1+\frac{\omega}{\omega_o}\right)^{-2.5}+\left(1-\frac{\omega}{\omega_o}\right)^{-2.5}-2\omega_0^{-2.5}\right) \quad (21)$$

Equation (21) is not immediately valid for the E_o edge because of the degeneracy of the valence band. However, one can apply it to the E_o edge if one neglects the field coupling between degenerate valence bands and uses appropriate average values of P^2 and μ_o. Each one of the three valence bands can be assumed to have a mass equal to three times the conduction band mass and a corresponding matrix element equal to $\frac{1}{3}p^2$ [48]. Hence eq (20) must be used with the matrix element P^2 and $\mu_o=\frac{3}{4}m_e$ if the three valence bands are to be included. The spin-orbit splitting Δ_o of the valence band is taken into account, if $\Delta_o \ll E_o$, by replacing ω_o by its average value $E_o+\frac{\Delta_o}{3}$. Since P^2 is almost the same for all materials of the germanium family, we can replace it by a typical value ≈ 0.4 (in atomic units). The values of μ_o and $\omega_o=E_o+\frac{\Delta_o}{3}$ for Ge, Si and GaAs are listed in table I. Using these numbers, eq (20) yields the values of $\chi^{(3)}_{1111}$ ($\omega=0$) listed in table II. While this contribution

TABLE I. *Values of the parameters required for the evaluation of the Franz-Keldysh contributions to $\chi^{(3)}_{1111}$. Frequencies in eV, a_o in Bohr radii, μ_o in units of the free electron mass. p^2 has been taken equal to 0.4 for all materials.*

	Ge	Si	GaAs
ω_g	4.3	4.8	5.2
ω_p	15.5	17.35	15.5
ϵ_o-1	11	15	10
μ_o	0.03	0.04	0.05
ω_o	0.9	4	1.5
a_o	10.7	10.3	10.7
ω_1	2.2	3.3	3.0

TABLE II. *Contribution of the various Franz-Keldysh effects discussed here to $\chi^{(3)}_{1111}$ and $\chi^{(3)}_{\xi\xi\xi\xi}$. In units of 10^{-10} e.s.u. Also, experimental values of the bound carrier contributions to $\chi^{(3)}_{1111}$ and $\chi^{(3)}_{\xi\xi\xi\xi}$.*

		E_g contribution	E_0 contribution	E_1 contribution	Experiment[57]
Ge	$\chi^{(3)}_{1111}$	0.26	0.67	0.20	1.0
	$\chi^{(3)}_{\xi\xi\xi\xi}$	0.26	0.67	0.26	1.5
Si	$\chi^{(3)}_{1111}$	0.22	0.00	0.27	0.06
	$\chi^{(3)}_{\xi\xi\xi\xi}$	0.22	0.00	0.36	0.08
GaAs	$\chi^{(3)}_{1111}$	0.12	0.087	0.045	0.12
	$\chi^{(3)}_{\xi\xi\xi\xi}$	0.12	0.087	0.060	0.10

is zero for Si and is not excessive in GaAs (it may, therefore, be assumed as included in the average gap calculation given above), it is dominant in Ge. In first approximation it may be added to the average gap calculation: excellent agreement with the experimental results is then found.

For InAs, with $\omega_o=0.5$ eV and $\mu=0.02$, we find from eq (20) $\Delta\chi^{(3)}_{1111}$ ($\omega=0$)$=7\cdot 10^{-10}$, which is of the order of the free-carrier contribution for the samples with the lowest electron concentrations measured ($N=2\cdot 10^{16}$ cm^{-3}) [57]. This is contrary to the statement found in the literature that for these carrier concentrations in InAs $\chi^{(3)}_{1111}$ is dominated by the free-carrier contribution [56,57,58].

The interband contribution of E_o to $\chi^{(3)}_{1111}$ for $\omega=0$ is easily obtained from the expression (see eq (8)):

$$\Delta\epsilon_r(\omega=0)=\frac{(2\mu_0)^{3/2}p^2}{2}\omega_g^{-3/2} \quad (22)$$

If one assumes that the repulsion produced by the field affects μ_o in the manner predicted by the $\mathbf{k}\cdot\mathbf{p}$ expression with constant matrix elements of $\mathbf{p}(\mu_o \propto \omega_g)$, the corresponding interband contribution to $\chi^{(3)}_{1111}$ vanishes. If, on the other hand, one assumes μ_o to be field independent one also finds a negative contribution to $\chi^{(3)}_{1111}$ about two orders of magnitude smaller than the Franz-Keldysh contribution, and hence negligible.

4.3. E_1 Critical Points

The E_1 optical structure is usually attributed to M_1 critical points along the {111} directions. While M_1 critical points are known to yield no contribution to $\chi^{(3)}_{1111}$ [52], there are M_o critical points of the same symmetry slightly below the M_1 critical points. This combination of M_o and M_1 critical points with a very large longitudinal mass, can actually be approximated by two-dimensional minima [48]. The contribution of one of these two-dimensional minima to the long-wavelength dielectric constant is (we assume four, and not eight equivalent {111} directions):

$$\Delta\epsilon_r=\frac{4\sqrt{3}\mu\perp p^2}{a_o\omega_1^2} \quad (23)$$

where a_o is the lattice constant and P^2 the appropriate square matrix element. We have tried to calculate the Franz-Keldysh contribution to $\chi^{(3)}_{1111}$ of these two-dimensional critical points in a way similar to that used above, but we have run into difficulties when evaluating the limits of the two-dimensional electro-optic functions for $\eta\rightarrow+\infty$. In view of this we have instead evaluated the effect of the three-dimensional M_o critical points, with the longitudinal effective mass replaced by the value required to give at long wavelengths a contribution to ϵ_r equal to that in eq (23).

Under these conditions, and because of the large longitudinal mass, only fields transverse to the critical point axis contribute to $\chi^{(3)}_{1111}$. When summing the contributions of the four equivalent valleys, it is found that the effect becomes anisotropic: the ratio of the third order susceptibility for $\mathscr{E}$ along {111} ($\chi^{(3)}_{\xi\xi\xi\xi}$), to that for $\mathscr{E}$ along {100} is 4/3. This argument is independent of the specific model chosen for the {111} transitions, provided $\mu_{||}\gg\mu_{\perp}$. It gives the type of anisotropy ($\chi^{(3)}_{\xi\xi\xi\xi}>\chi^{(3)}_{1111}$) observed for Ge and Si, but not for GaAs [57]. The Franz-Keldysh contribution of E_1 to $\chi^{(3)}_{1111}$ as found by the procedure sketched above, is:

$$\Delta\chi^{(3)}_{1111}=0.52\frac{p^2}{a_o\omega_1^5} \quad (24)$$

or, with ω_1 in eV and $\chi^{(3)}_{1111}$ in e.s.u.:

$$\Delta\chi^{(3)}_{1111}=2.7\cdot 10^{-8}\frac{p^2}{a_o\omega_1^5} \quad (25)$$

(a_o in Bohr radii and P^2 in atomic units.)

The matrix element P should have approximately the same value as for the E_o gap. In order to take care of the spin-orbit splitting Δ_1 of E_1 we substitute ω_1 by $E_1+\Delta_1/2$. The approximate values of a_o, and ω_1 for Ge, Si and GaAs are listed in table I. The values calculated for the Franz-Keldysh contribution to E_1 to $\chi^{(3)}_{1111}$ and $\chi^{(3)}_{\xi\xi\xi\xi}$ are listed in table II. While the calculated anisotropy has, for Ge and Si, the sign observed experimentally, its magnitude is far too small to explain the experimental anisotropy, especially after the E_o and the E_g contributions are added. There is a possibility that the E_1 contribution of eq (25) may have been underestimated. Exciton quenching effects [59,60], not included in our calculation, may increase this contribution.

We cannot offer even a qualitative explanation of the sign of the $\chi^{(3)}$ anisotropy observed for GaAs. It would be interesting to determine, through measurements of other III−V or II−VI compounds, whether it is connected with the lack of inversion symmetry in these materials.

The interband contribution of the E_1 edges can be evaluated in a manner analogous to that used for the E_o and the ω_g gaps. We also find that this contribution is negative and, typically, two orders of magnitude below the Franz-Keldysh contribution.

5. Acknowledgments

I am indebted to Drs. Buss, Kane, Phillips, Van Vechten, and Aspnes for sending preprints of their work, prior to publication and to the staff of DESY for their hospitality.

6. References

[1] Cohen, M. L., and Bergstresser, T. K., Phys. Rev. **141**, 789 (1966).
[2] Cardona, M., and Pollak, F. H., Phys. Rev. **142**, 530 (1966).
[3] Dresselhaus, G., and Dresselhaus, M. S., Phys. Rev. **160**, 649 (1967).

[4] Herman, F., Kortum, R. L., Kuglin, C. D., and Shay, J. L., in "II—VI Semiconducting Compounds," D. G. Thomas, ed., (W. A. Benjamin, New York, 1967), p. 503.
[5] Gilat, G., and Dolling, G., Phys. Letters **8**, 304 (1964); Gilat, G., and Raubenheimer, L. J., Phys. Rev. **144**, 390 (1966).
[6] Higginbotham, C. W., Pollak, F. H., and Cardona, M., Proceedings of the IX International Conference on the Physics of Semiconductors, Moscow 1968 (Publishing House Nauka, Leningrad, 1968) p. 57.
[7] Buss, D. D., and Parada, N. J., private communication; see also article by D. D. Buss and V. E. Shirf in these proceedings.
[8] Kane, E. O., Phys. Rev. **146**, 558 (1966).
[9] Philipp, H. R., and Ehrenreich, H., Phys. Rev. **129**, 1550 (1963).
[10] Cardona, M., Z. Physik **161**, 99 (1961).
[11] Zhang, H. I., and Callaway, J., Phys. Rev. **181**, 1163 (1969).
[12] Walter, J. P., and Cohen, M. L., Phys. Rev., to be published.
[13] Seraphin, B. O., and Bottka, N., Phys. Rev. **145**, 628 (1966).
[14] Shaklee, K. L., Rowe, J. E., and Cardona, M., Phys. Rev. **174**, 828 (1968).
[15] Matatagui, E., Thompson, A. G., and Cardona, M., Phys. Rev. **176**, 950 (1968).
[16] Higginbotham, C. W., Ph. D. Thesis, Brown University, 1969.
[17] Eckelt, P., Madelung, O., and Treusch, J., Phys. Rev. Letters **18**, 656 (1967).
[18] Brinkman, W., and Goodman, B., Phys. Rev. **149**, 597 (1966).
[19] Pollak, F. H., Cardona, M., Higginbotham, C. W., Herman, F., and Van Dyke, J. P., Phys. Rev., to be published.
[20] McElroy, P., Ph. D. Thesis, Harvard University, 1968.
[21] Cardona, M., and Greenaway, D. L., Phys. Rev. **133**, A1685 (1964).
[22] Scanlon, W. W., J. Phys. Chem. Solids **8**, 423 (1959).
[23] Aspnes, D. E., and Cardona, M., Phys. Rev. **173**, 714 (1968).
[24] Sandrock, R., Phys. Rev. **169**, 642 (1968).
[25] Tutihasi, S., and Chen, I., Phys. Rev. **158**, 623 (1967).
[26] Lin, P. J., and Phillips, J. C., Phys. Rev. **147**, 469 (1966).
[27] Wiech, G., in "Soft X-Ray Spectra," D. J. Fabian, ed., (Academic Press, New York, 1968) p. 59.
[28] Feuerbacher, B., Skibowski, M., Godwin, R. P., and Sasaki, T., JOSA **58**, 1434 (1968).
[29] See for instance R. S. Knox, "Theory of Excitons," (Academic Press, N.Y., 1963).
[30] Mahan, G. D., Phys. Rev. Letters **18**, 448 (1967).
[31] Velicky, B., and Sak, J., Phys. Status Solidi **16**, 147 (1966).
[32] Kane, E. O., Phys. Rev. **180**, 852 (1969).
[33] Marple, D. T. F., and Ehrenreich, H., Phys. Rev. Letters **8**, 87 (1962).
[34] Cardona, M., J. Appl. Phys. **36**, 2181 (1965).
[35] Inoue, M., Okazaki, M., Toyozawa, Y., Inui, T., and Nanamura, E., Proc. Phys. Soc. Japan **21**, 1850 (1966).
[36] Hermanson, J., Phys. Rev. **150**, 660 (1966).
[37] Shaklee, K. L., Ph. D. Thesis, Brown University, 1969.
[38] Penn, D., Phys. Rev. **128**, 2093 (1962).
[39] Srinivasan, G., Phys. Rev. **178**, 1244 (1969).
[40] Nara, H., J. Phys. Soc. Japan **20**, 778 (1965).
[41] Van Vechten, J. A., Phys. Rev. **182**, 891 (1969). In this reference a correction factor of the order of unity is added to eq (6) so as to take the polarizability of the core d electrons into account.
[42] Phillips, J. C., Phys. Rev. Letters **20**, 550 (1968).
[43] Phillips, J. C., Covalent Bonding in Molecules and Solids (University of Chicago Press, Chicago) to be published.
[44] Phillips, J. C., and Van Vechten, J. A., Phys. Rev. **183**, 709 (1969); Levine, B. F., Phys. Rev. Letters **22**, 787 (1968).
[45] Cardona, M., Paul, W., and Brooks, H., J. Phys. Chem. Solids **8**, 204 (1959).
[46] Korovin, L. I., Soviet Phys. Solid State **1**, 1202 (1959).
[47] Cardona, M. in "High Energy Physics, Nuclear Physics, and Solid State Physics," I. Saavedra, ed., (W. A. Benjamin, New York, 1968).
[48] Higginbotham, C. W., Cardona, M., and Pollak, F. H., Phys. Rev. **184**, 821 (1969).
[49] De Meis, W. M., Technical Report No. HP-15 (ARPA-16), Harvard University (1965).
[50] Shileika, A. Yu., Cardona, M., and Pollak, F. H., Solid State Communications **7**, 1113 (1969).
[51] Yu, P. Y., to be published.
[52] Van Vechten, J. A., and Aspnes, D. E., Phys. Letters, in press.
[53] Aronov, A. G., and Pikus, G. E., Proceedings of the IX International Conference on the Physics of Semiconductors, Moscow, 1968, (Publishing House Nauka, Leningrad, 1968), p. 390.
[54] Cardona, M., "Modulation Spectroscopy," F. Seitz, D. Turnbull, and H. Ehrenreich, eds., (Academic Press Inc., New York, N.Y.).
[55] Antonsiewicz, H. A., in "Handbook of Mathematical Functions," (M. Abramowitz and I. A. Stegun, eds.) (Dover Pub. Inc., New York, N.Y., 1965) p. 448.
[56] Wolff, P. A., and Pearson, G. A., Phys. Rev. Letters **17**, 1015 (1966).
[57] Wynne, J. J., Phys. Rev. **178**, 1295 (1969).
[58] Patel, C. K. N., Slusher, R. F., and Fleury, P. A., Phys. Rev. Letters **17**, 1011 (1966).
[59] Hamakawa, Y., Germano, F. A., and Handler, P., J. Phys. Soc. Japan, Suppl. **21**, 111 (1966).
[60] Shaklee, K. L., Rowe, J. E., and Cardona, M., Phys. Rev. **174**, 828 (1968).

(Paper 74A2-597)